AIAA JOURNAL
Vol. 39, No. 4, April 2001

Computation of Rarefied Gas Flows Around a NACA 0012 Airfoil

Jing Fan,* Iain D. Boyd,† and Chun-Pei Cai‡
University of Michigan, Ann Arbor, Michigan 48109
and
Konstantinos Hennighausen§ and Graham V. Candler¶
University of Minnesota, Minneapolis, Minnesota 55455

Rarefied gas flows around a NACA 0012 airfoil are simulated using both particle and continuum approaches. Three different conditions are considered: supersonic, transonic, and low subsonic. In all three cases, the continuum approach solves the Navier–Stokes equations with a slip boundary condition on the airfoil surface. For the supersonic and transonic cases, the particle method employed is the direct simulation Monte Carlo method. Because of problems with this method at the low subsonic condition, caused by excessive statistical fluctuations, a new particle method called the information preservation technique is applied. The computed density and velocity flowfields are compared with experimental data and found to be in generally good agreement. Some interesting features in the surface pressure distributions along the airfoil are found for these low-Reynolds-number flows.

Introduction

THERE is great interest in the development of very small aircraft, such as the micro air vehicle (MAV) for a number of applications.[1] Most of the current MAVs are scaled-down versions of conventional aircraft, with some researchers employing flapping wings. Basic studies are required to understand the aerodynamics appropriate to MAVs. Present day MAVs experience low Reynolds number flows characterized by chord lengths of a few centimeters. There is interest in developing even smaller vehicles in the future, and at some stage, the characteristic length scale will be sufficiently small that noncontinuum, rarefied flow phenomena will become prevalent. Hypersonic rarefied gas flows have been widely studied over the past 40 years, primarily for aerospace applications such as reentry problems. Rarefied gas flows involved in microvehicles, however, are at low or moderate Mach numbers. The fundamental fluid mechanics and aerodynamics under such conditions are not well understood.

In this paper, we study rarefied gas flows around a NACA 0012 airfoil using particle and continuum approaches. This type of airfoil is of a basic shape and is appropriate as a starting point to study the aerodynamic features of microvehicles. Three Mach numbers are considered: 2.0, 0.8, and 0.1. There are experimental data available to compare at Mach 2 and 0.8, where rarefaction occurs primarily due to low-density flow over a 4-cm-chord-length airfoil.[2,3] Previous work found that there was a significant difference between Navier–Stokes and experimental density fields.[2,4] It was explained by the existence of a slip velocity along the airfoil surface that was not considered in the Navier–Stokes calculations. A further investigation at Mach 2.0 and zero angle of attack showed that this difference may be considerably reduced when the slip velocity and temperature jump were included in the calculations.[3,5] Model equations of the Boltzmann equation, such as the Bhatnagar–Gross–Krook (BGK) model[6] for monatomic gases and the Morse[7]–Holway[8] model for gases with internal degrees of freedom, were also used to simulate the Mach 2.0 flows.[5] The density field given by the Morse–Holway model compared better with the experiment than that given by the BGK model.

In the present study, the continuum approach solves the Navier–Stokes equations with a slip boundary condition on the airfoil surface. For the supersonic and transonic cases, the particle approach employed is the direct simulation Monte Carlo (DSMC) method.[9] Because of problems with this method at the low subsonic condition, caused by excessive statistical fluctuations, a new particle method called the information preservation (IP) technique[10] is applied.

Received 1 December 1999; revision received 15 August 2000; accepted for publication 28 August 2000.

*Research Associate, Department of Aerospace Engineering.
†Associate Professor, Department of Aerospace Engineering.
‡Graduate Research Assistant, Department of Aerospace Engineering.
§Graduate Research Assistant, Department of Aerospace Engineering and Mechanics.
¶Professor, Department of Aerospace Engineering and Mechanics.

Particle Approach

As the primary computational tool for analyzing rarefied gas flows, the DSMC method has been widely used in the engineering context.[11] A main handicap of this method is the requirement of a large number of samples to reduce the statistical scatter in simulation of low-speed flows. Such a simulation is extremely time consuming and beyond the capabilities of current computers.[11]

To solve this problem, the IP technique was proposed.[10] The basic premise of this technique is to associate both microscopic and macroscopic information with each particle in a computer simulation. The usual DSMC steps are applied to the microscopic properties, and simple conservation laws are applied to the macroscopic properties. Macroscopic quantities are obtained through time or ensemble averaging of the information. This technique has been successfully used to simulate unidirectional low-speed flows (1 cm/s–1 m/s) such as Couette flows, Poiseuille flows, and Rayleigh flows (see Ref. 10). The meaningful velocity and surface shear stress distributions were obtained with a sample size of 10^3–10^4 that was four orders of magnitude smaller than that required by DSMC (about 10^8). Therefore, there was a tremendous reduction in CPU time.

To clarify why the IP method works, let us compare the formulas used by DSMC and IP to compute a macroscopic velocity $\boldsymbol{U}_\ell$ in a cell. Consider a uniform flow with velocity $\boldsymbol{u}_k$. The DSMC formula is

$$\boldsymbol{U}_\ell = \frac{1}{N}\sum_{k=1}^{N} \boldsymbol{c}_k = \boldsymbol{u}_k + \frac{1}{N}\sum_{k=1}^{N} \boldsymbol{c}_t, k \tag{1}$$

and the IP formula is

$$\boldsymbol{U}_\ell = \frac{1}{N}\sum_{k=1}^{N} \boldsymbol{u}_k = \boldsymbol{u}_k \tag{2}$$

where N is the sample size of simulated particles in the cell and $\boldsymbol{c}_k$ is the velocity of a simulated particle. According to kinetic theory, $\boldsymbol{c}_k$ consists of two parts: the thermal part $\boldsymbol{c}_{t,k}$ and macroscopic part $\boldsymbol{u}_k$. The DSMC method stores $\boldsymbol{c}_k$ and uses it to compute the particle trajectory and $\boldsymbol{U}_\ell$ according to Eq. (1). The IP method stores both $\boldsymbol{c}_k$ and $\boldsymbol{u}_k$. It uses the former to compute the particle trajectory and uses the latter to compute $\boldsymbol{U}_\ell$ according to Eq. (2). Note that the macroscopic velocity given by the IP formula (2) is the exact value

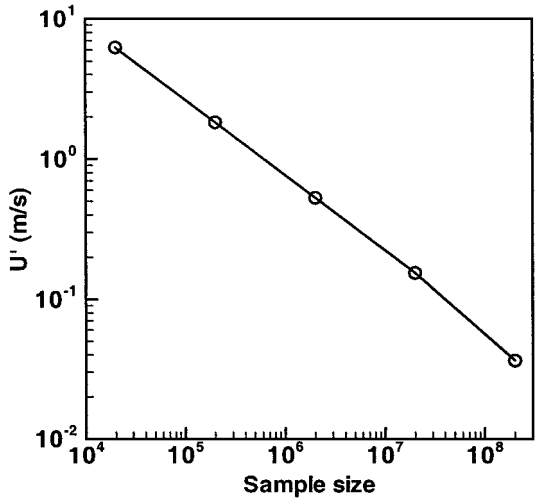

Fig. 1 Statistical scatter vs sample size in DSMC simulation of a stationary homogeneous argon gas at 273 K; U' is the x-component amplitude of the macroscopic velocity fluctuation caused by the statistical scatter.

$\boldsymbol{u}_k$ of for any sample size, whereas there is an explicit fluctuation term

$$\frac{1}{N}\sum_{k=1}^{N}\boldsymbol{c}_{t,k}$$

in the DSMC formula (1) that decreases with the square root of the sample size of N.

For low-speed flows, because of the small ratio of macroscopic to thermal velocity, it is difficult to reduce

$$\frac{1}{N}\sum_{k=1}^{N}\boldsymbol{c}_{t,k}$$

to an acceptable level. A clear demonstration of this is shown in Fig. 1, where U' is the x-component amplitude of the macroscopic velocity fluctuation caused by

$$\frac{1}{N}\sum_{k=1}^{N}\boldsymbol{c}_{t,k}$$

in DSMC simulation of a stationary homogeneous argon gas at temperature 273 K. For example, U' is 53 cm/s at a sample size of 2×10^6, which is unacceptable for many low-speed applications such as microchannel flows where the experimental inflow velocity was about 20 cm/s (Refs. 12–14). Further increase of the sample size is beyond the capabilities of current computers, particularly for multidimensional flows.

In contrast to the DSMC method, the IP technique has proven very effective in reducing statistical scatter in simulating one-dimensional benchmark flows.[10] Meaningful results were obtained with a sample size of 10^3-10^4, even when the flow velocity was of order 1 cm/s. This technique is also applicable to multidimensional flows. An implementation of the method may be summarized as follows:

1) Assign each simulated particle an information velocity $\boldsymbol{u}_i$, density ρ_i, temperature T_i, and a thermal velocity $\boldsymbol{c}_i$. Assign each cell a macroscopic velocity $\boldsymbol{U}_\ell$, density ρ_ℓ, and temperature T_ℓ.

2) Initially, set $\boldsymbol{U}_\ell$, ρ_ℓ, and T_ℓ of a cell according to the initial flow conditions, and set $\boldsymbol{u}_i$, ρ_i, and T_i of all simulated particles in the cell to be equal to $\boldsymbol{U}_\ell$, ρ_ℓ, and T_ℓ.

3) Move simulated particles according to the thermal velocities using the same algorithms and models as the DSMC method described in detail in Ref. 9.

4) In a time step Δt, the information velocity of a simulated particle may be changed because of the following reasons:

a) It may be changed because of impact with a wall. Set the reflected information velocity in accordance with the statistical behavior of an enormous number of real molecules. For example, it is equal to the wall velocity for a diffuse reflection surface.

b) It may be changed because of entry into the computational domain from the outer boundaries. Set the information velocity in accordance with the boundary conditions.

c) It may be changed because of acceleration by external forces. The sum of the forces acting on the ℓth cell is

$$\boldsymbol{F}_\ell=\sum_{k=1}^{2\phi}p_\ell^k\Delta A_\ell^k\boldsymbol{n}_\ell^k+\boldsymbol{f}_\ell^k\Delta V_\ell \tag{3}$$

where $\boldsymbol{p}_\ell^k$ is the gas pressure acting on the kth surface of the ℓth cell with area ΔA_ℓ^k and normal direction $\boldsymbol{n}_\ell^k$, ϕ is the flow dimension, and $\boldsymbol{f}_\ell^k$ is the volume force acting on the cell with volume ΔV_ℓ. Here $\boldsymbol{p}_\ell^k$ is computed using the pressures of the cells with the kth surface. The cell pressures are calculated from the stored ρ_ℓ and T_ℓ using the ideal gas equation of state. An acceleration thus generated is

$$\boldsymbol{a}_\ell=\boldsymbol{F}_\ell/\rho_\ell\Delta V_\ell \tag{4}$$

which will contribute a velocity increment $\boldsymbol{a}_\ell\Delta t$ to every simulated particle in the cell during the time step.

d) Information velocity may be change because of collision with other particles. A simple scheme is employed to distribute postcollision information velocities of two simulated particles

$$\boldsymbol{u}_{i,1}'=\boldsymbol{u}_{i,2}'=\frac{m_1\boldsymbol{u}_{i,1}^*+m_2\boldsymbol{u}_{i,2}^*}{m_1+m_2} \tag{5}$$

where superscripts * and' denote pre- and postcollision, respectively. An alternative scheme is to keep the information velocities unchanged during the collision process. Both of these were tested in simulation of Couette flows, Poiseuille flows, and Rayleigh flows and gave identical results. This is easily understood because the scattering of the thermal velocities during the collision process is isotropic in the center of mass frame of reference according to the variable hard sphere model[9,15] that is used to describe the interaction between simulated particles. Such an isotropic scattering makes schemes that satisfy momentum conservation the same in the statistical aspect.

5) Update $\boldsymbol{U}_\ell$, ρ_ℓ, and T_ℓ at each time step:

$$\boldsymbol{U}_\ell=\sigma\boldsymbol{U}_{\text{new}}+(1-\sigma)\boldsymbol{U}_{\text{old}} \tag{6}$$

where σ is a relaxation factor ranging between 0 and 1, $\boldsymbol{U}_{\text{old}}$ is the value of $\boldsymbol{U}_\ell$ at the last time step, $\boldsymbol{U}_{\text{new}}$ is the arithmetic mean of the information velocities of all the simulated particles in the cell during this time step

$$\boldsymbol{U}_{\text{new}}=\frac{\sum_{k=1}^{N}m_k\boldsymbol{u}_k}{\sum_{k=1}^{N}m_k} \tag{7}$$

where m is the particle mass. For a large N, σ may be set to 1:

$$\rho_\ell=\rho_{\text{old}}+\Delta\rho \tag{8}$$

where ρ_{old} is the value at the last time step and $\Delta\rho$ is the density variation during this time step. According to the continuity equation, $\Delta\rho$ may be written as

$$\Delta\rho=-\frac{\Delta t}{\Delta V_\ell}\sum_{k=1}^{2\phi}\rho_\ell^k\boldsymbol{U}_\ell^k\boldsymbol{n}_\ell^k\Delta A_\ell^k \tag{9}$$

where ρ_ℓ^k and $\boldsymbol{U}_\ell^k$ are the macroscopic density and velocity across the kth surface of the ℓth cell, respectively. They can be obtained through an average of the macroscopic velocities and densities of the cells with the kth surface.

A technique to update T_ℓ is under study. At this stage, we employ the isothermal assumption. Low-speed flows may be categorized into those types with and without external heating. Analysis shows that the isothermal assumption is valid for the type without external heating.[16] Recent experiments on rarefied low-speed flows in

microchannels solidly supported this analysis.[12–14] Many flows involved in current micro-mechanical-electro systems, including low subsonic flow past airfoils of interest in this paper, fall into this category.

6) Update the information densities of all the simulated molecules in the ℓth cell

$$\rho_i = \rho_\ell \tag{10}$$

7) Compute macroscopic quantities through statistical averaging of the information quantities. The shear stress and pressure on a surface element with area ΔA_w during the sampling interval t_s are given by

$$\tau_w = \frac{\sum_{j=1}^{N_w} m_j \left(u_{\tau,j}^{\text{in}} - u_{\tau,j}^{\text{re}}\right)}{t_s \Delta A_w}, \qquad p_w = \frac{\sum_{j=1}^{N_w} \rho_j R T_j^{\text{in}}}{N_w} \tag{11}$$

where N_w is the total number of molecules hitting the element during t_s, subscript τ denotes the tangential direction of the element, and superscripts in and re denote the values before and after striking the element, respectively.

The macroscopic velocity is the arithmetic mean of information velocities of all sampling particles in the cell during t_s and is obtained using Eq. (2). The macroscopic density is solved similarly.

8) For steady flows, repeat steps 3–6 until the flow reaches a steady state. Then repeat steps 3–7 to sample. For unsteady flows, repeat steps 2–7 until the end of the evolution period.

Continuum Approach

Because of the computational expense of particle methods (DSMC), we seek to use such techniques only where necessary. In addition, at low speeds, particle methods suffer from statistical scatter error because the bulk velocity becomes small relative to the thermal velocity. Hence, we consider numerical solutions of the Navier–Stokes equations, incorporating appropriate slip boundary conditions, and assess their applicability to the current flow regimes by comparing to the DSMC results.

The Navier–Stokes equations are solved about a NACA 0012 airfoil on a two-dimensional finite volume grid using the implicit Gauss–Seidel line relaxation method[17] and second-order accurate modified Steger–Warming flux vector splitting (see Ref. 18). A structured, elliptically generated C grid provides the computational domain. The grid conforms to the airfoil surface and extends to a semicircular upstream boundary and a rectangular wake boundary. To resolve adequately the viscous flowfield, we use a grid of 300 cells in the airfoil-conforming direction and wake and 100 cells in the wall-normal direction. Cells are concentrated in the near-body region and in the wake to capture properly the shear-layer physics, which dominate this flow regime. For the 10-deg angle-of-attack solution, we rotate the airfoil about its trailing edge to align properly the grid with the wake region.

At the outer edge of the computational grid, 10 chords from the airfoil surface, we apply freestream conditions. Under the conditions of interest, the gas is rarefied, and the conventional no-slip boundary condition does not necessarily hold. Instead, we use the Maxwell–Smoluchowski slip boundary conditions that allow for the presence of an imperfect momentum and energy accomodation at the surface[19]:

$$u_{\text{slip}} = \frac{2-\sigma_v}{\sigma_v} \frac{1}{\rho (2RT_w/\pi)^{\frac{1}{2}}} \tau_s + \frac{3}{4} \frac{Pr(\gamma-1)}{\gamma R \rho T_w} (-q_s) \tag{12}$$

$$T_{\text{gas}} - T_w = \frac{2-\sigma_t}{\sigma_t} \frac{2(\gamma-1)}{\gamma+1} \frac{1}{R\rho (2RT_w/\pi)^{\frac{1}{2}}} (-q_n) \tag{13}$$

where σ_v and σ_t are the momentum and energy accomodation coefficients (set to unity in all of the computations presented here), q_n and q_s are the gas normal and tangential heat transfer rates, T_w is the wall temperature, ρ is density, τ_s is the wall viscous stress component due to skin friction, R is the gas constant, γ is the ratio of specific heats, and Pr is the Prandtl number.

Computational Domain Overlay Technique

Far-field computational boundary conditions for external subsonic flows are an issue that the DSMC method needs to treat carefully. This method has been primarily used to study hypersonic flows where the freestream conditions are applicable to far-field boundaries not far from the body. However, these simple conditions cannot be used for subsonic flows. In principle, there are two means to address the issue. One is to impose the freestream conditions at the far-field boundaries and locate them quite far away from the region of interest to minimize any inconsistent effects. Another is to locate the far-field boundaries at a near distance from the primary region of interest to limit the computational domain and describe the boundary conditions using models that are a function of local physical quantities and gradients, etc. The latter is not suitable to the DSMC method because it is difficult to immediately compute the local physical quantities and gradients. Application of the former approach to the DSMC method encounters a computational difficulty that needs to be considered.

As with most direct methods, the numerical expense of the DSMC method is high, thus requiring careful attention to be paid to the computational efficiency, particularly for subsonic flows where a large number of samples are required to resolve the flowfields varying in a narrow range. The small cell size that is often necessary in a region near the body where the flows have relatively large gradients is unfeasible for a large computational domain, because the DSMC expense is proportional to $(L/\Delta l)^{\phi}$, where L is the characteristic length of Ω_D, Δl is the cell size, and ϕ is the flow dimension. Variable cell size is inefficient because there will be too many simulated particles in the large cells to be computationally efficient when the number of simulated particles in the small cells is at an appropriate level. The weighting factor technique, which can distribute the number of simulated particles uniformly over the cells, is also not suitable because the accompanied random walk is deleterious to obtaining statistically converged solutions.

A computational domain overlay technique is proposed to alleviate the aforementioned difficulties. First, a large computational domain and large cell size are used. To satisfy the requirement that the distance between a collision pair be smaller than the mean free path, the subcell technique is employed.[9] Then the cells are subdivided into a set of subcells (the subcell size is required to be smaller than the mean free path), and collision pairs are selected within the subcells. The large cells may resolve the flowfield distant from the body where the flow gradients are small, though they are not fine enough to describe the flow structure near the body. Then the number density, velocity, and temperature along a locus are extracted from the computation with the large computational domain and cell size. The locus is chosen to be as close to the body as possible on the premise that the surrounding flowfield can be resolved by the large cell size. Next, the locus is used as the far-field boundary of a new calculation with smaller cells.

Results and Discussion

Consider four cases of airflows around a NACA 0012 airfoil. The chord length L_c is 0.04 m, and the freestream conditions are given in Table 1, where α denotes the angle of attack, $Re_\infty = V_\infty L_c/v$, $Kn_\infty = \lambda_\infty/L_c$, and the other symbols are defined as usual. To compare with measured data at Mach 2 and 0.8 (Refs. 2 and 3), cases A, B, and C employ the same conditions as the experiment.

DSMC calculations are carried out using a software system called MONACO,[20] which has been developed to incorporate the IP technique. The calculations employ an unstructured triangular grid. The

Table 1 Freestream conditions[a]

Case	M_∞	Re_∞	α, deg	ρ_∞, kg/m^3	T_∞, K	V_∞, m/s	Kn_∞
A	2.0	106	0	6.026×10^{-5}	161	509	0.026
B	2.0	106	10	6.026×10^{-5}	161	509	0.026
C	0.8	73	0	1.116×10^{-4}	257	257	0.014
D	0.1	19	0	1.315×10^{-4}	290	34	0.013

[a]Wall temperature is 290 K for all of the cases that are equal to the stagnation temperature.

Table 2 DSMC and IP computational parameters

Case	Ω_D	N_{cell}	Δl_s, m	Δt
A	$(-0.2, 2.5) \times (0, 2.5)$	43,597	1.3×10^{-4}	7×10^{-7}
B	$(-0.2, 2.5) \times (-2.5, 2)$	69,553	1.3×10^{-4}	7×10^{-7}
C	$(-5, 6) \times (0, 5)$	90,342	1.7×10^{-4}	8×10^{-7}
D	$(-10, 2.5) \times (0, 2.5)$	34,802	5.0×10^{-4}	2×10^{-7}

distance between a collision pair is limited to be smaller than the mean free path using the subcell technique.[9] Analyses showed that if collision pairs are selected directly within cells and the cell size is greater than the free mean path, the numerical errors of viscosity and thermal conductivity due to the finite cell size are not negligible.[21,22] Our studies found, however, that by utilizing the subcell technique, they would be negligible even when the cell size was much greater than the mean free path.

About 2×10^6 simulated particles are used in the DSMC and IP calculations. Other computational parameters are given in Table 2, where $\Omega_D = (x_1, x_2) \times (y_1, y_2)$ is a rectangular computational domain normalized by the chord length, N_{cell} is the number of cells, Δl_s is the subcell size, and Δt is the time step. The airfoil surface is assumed to be fully diffuse. At the far-field boundaries, the freestream conditions are applied to the supersonic cases, and the computational domain overlay technique is applied to the transonic case. For the low subsonic case, the freestream conditions are applied at the inlet, and zero-gradient conditions are used in the normal direction at the upper boundary and outlet.

The Navier–Stokes simulations use an inviscid calculation as an initial condition before the viscous terms are added to the calculation. For the inviscid calculations, Courant–Friedrichs–Lewy numbers on the order of 100 are used. Even though the implicit method includes a linearization of the normal-direction viscous terms, when the viscous terms are included the stable time step decreases by at least four orders of magnitude. This is a result of the very low Reynolds numbers of the simulations and makes these calculations very time consuming.

Case A: $M_\infty = 2, Re_\infty = 1.06 \times 10^2, \alpha = 0$ Degrees

Case A represents a high-speed, convection dominated flow. Although viscous effects play a greater role than they would in a conventional, high Reynolds number flight, they do not dominate the fluid motion. Because of the high freestream velocity, the DSMC method does not face the problems of statistical scatter that make low-speed calculations difficult. Similarly, the Navier–Stokes calculation converges well.

Figures 2 and 3 present the computed density and velocity fields, together with the experimental results.[2,3] Both DSMC and slip Navier–Stokes results show good agreement with the experiment in the bow shock and stagnant regions; in detail, the DSMC results are closer to the experiment. For instance, there is a contour with the value of 0.9 above the trailing edge in the DSMC and experimental velocity fields, but not in the Navier–Stokes velocity field.

Figure 4 compares the surface pressure coefficient distributions given by the DSMC method, the Navier–Stokes slip model, the Morse–Holway model, and the nonslip Navier–Stokes solution.[5] The surface pressure coefficient is defined as

$$C_p = \frac{2(p_w - p_\infty)}{\rho_\infty V_\infty^2} \tag{14}$$

The DSMC and Morse–Holway solutions are in excellent agreement, and the slip Navier–Stokes solution is closer to them than the nonslip solution.

Case B: $M_\infty = 2, Re_\infty = 1.06 \times 10^2, \alpha = 10$ Degrees

Like case A, case B represents a high-speed, convection dominated flow, but with a nonzero angle of attack. Figure 5 presents the DSMC, slip Navier–Stokes, and experimental density contours that agree well with each other. Figure 6 shows the DSMC and slip Navier–Stokes surface pressure distributions. Because of the nonzero angle of attack, there is a gap between the pressures acting

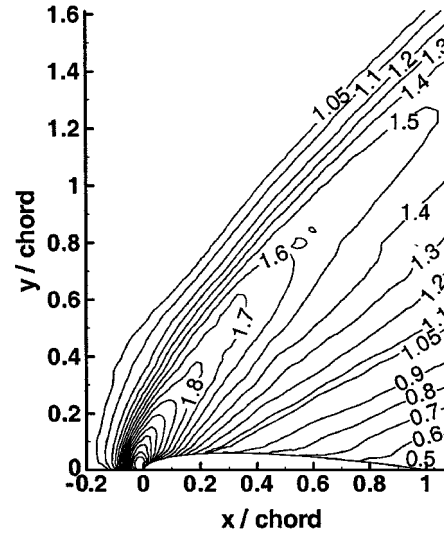

a) DSMC

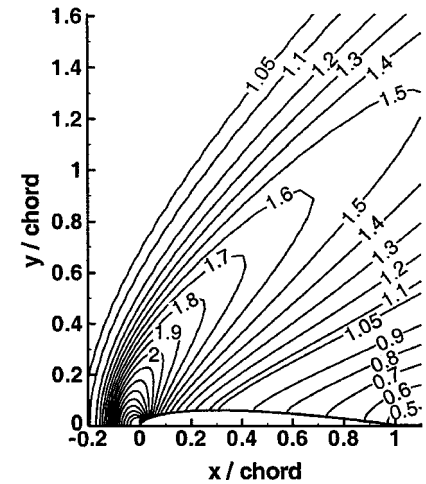

b) Slip N–S

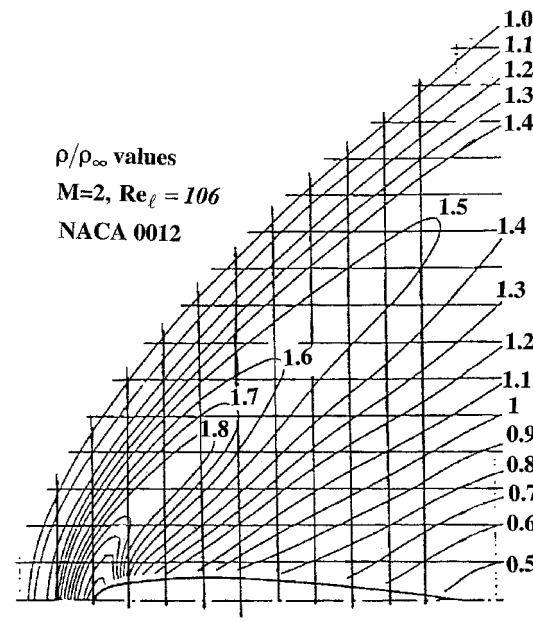

c) Experiment[2]

Fig. 2 Comparison of DSMC, slip Navier–Stokes (N–S), and experimental density fields ρ/ρ_∞ for case A.

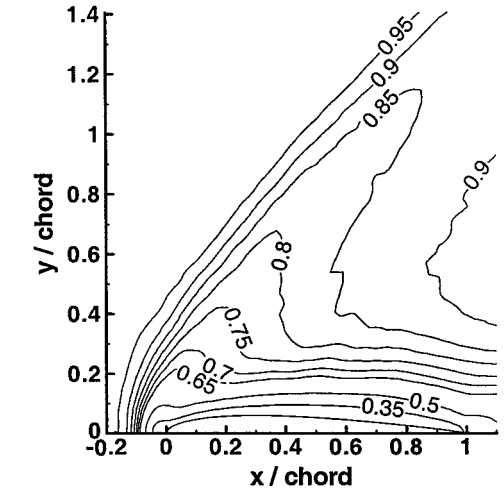

a) DSMC

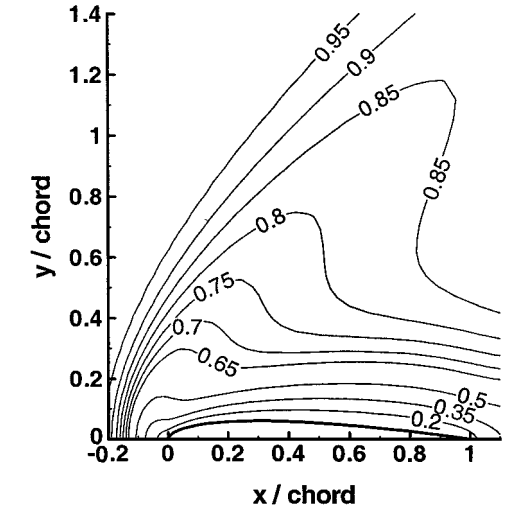

b) Slip N–S

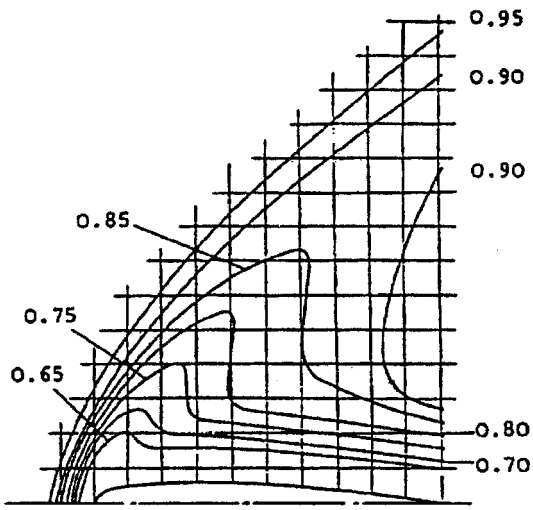

c) Experiment[3]

Fig. 3 Comparison of DSMC, slip N–S and experimental velocity fields V/V_∞ for case A.

on the lower and upper surfaces. The DSMC and Navier–Stokes gap sizes are close, whereas the Navier–Stokes results indicate a consistently higher pressure. The latter is considered to be caused by the rarefaction effects at the airfoil surface, though the Knudsen number based on the chord length is only 0.026. It is known that such an overall Knudsen number may make a misleading prediction about local conditions.[9] A gradient-length local (GLL) Knudsen number based on the density gradient[23]

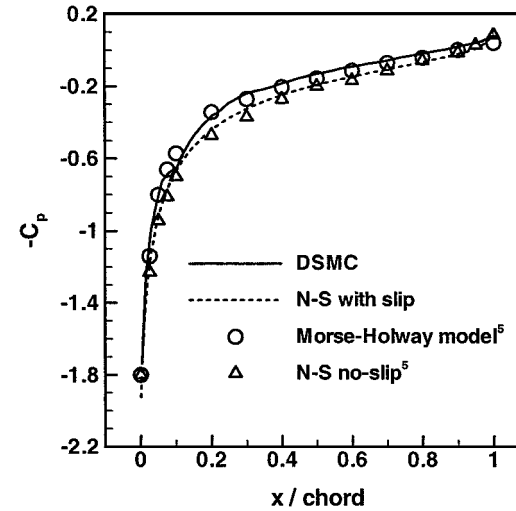

Fig. 4 Comparison of surface pressure distributions between different computational approaches for case A.

$$Kn_{\mathrm{GLL}} = \lambda|\Delta\rho|/\rho \tag{15}$$

is computed using the slip Navier–Stokes solution (Fig. 7). Comparison between DSMC and Navier–Stokes results for shock waves and hypersonic flows around a sphere showed that the continuum approach broke down wherever Kn_{GLL} exceeds 0.05 (Ref. 23). Application of this critical value to Fig. 7 indicates that the continuum approach is invalid in a core of the bow shock wave and in the region adjacent to the airfoil surface.

Case C: $M_\infty = 0.8$, $Re_\infty = 7.3 \times 10^1$, $\alpha = 10$ Degrees

Case C, a transonic flow, involves a flowfield of elliptic character, presenting difficulties with the boundary conditions at the outer edge of the domain. In the Navier–Stokes computation, we apply freestream conditions at the outer edge, 10 lengths from the airfoil, which has been shown to be a sufficiently large domain not to affect the near airfoil flow. In the DSMC calculation, we employ the domain overlay technique discussed earlier. A computation based on a domain of $(-10L_c, 11L_c) \times (0, 10L_c)$ and a cell size of about 5 λ is performed first. The flow density, temperature, and velocity are extracted along a locus of $(-5L_c, 6L_c) \times (0, 5L_c)$. In a new calculation with this locus as the outer boundary edge, the extracted flow properties are used as the boundary conditions. They are found to be different from the freestream conditions, particularly in regions close to the symmetry line of the airfoil. Moreover, the density field based on the extracted boundary conditions compares better with the experiment[2] than that based on the freestream conditions.

Figure 8 presents the DSMC and slip Navier–Stokes density fields, together with experimental data.[2] The DSMC calculation takes about 400 CPU hours on an SGI OCTANE workstation and the sample size is about 400,000 in each cell. However, the statistical scatter is clearly seen in Fig. 8a that makes the contours fluctuate in comparison with the Navier–Stokes and experimental contours. Although both calculated density distributions exhibit the same general features as the experiment, there are regions of significant difference in detail. For instance, the experimental density varies little from 0.995 to 1.005 in a large region originating from the airfoil surface, whereas the DSMC and Navier–Stokes densities vary from about 0.92 to 1.02 and from 0.94 to 1.04, respectively. This difference perhaps results from the tunnel wall in the experiment that has a diameter of order 10 cm (Ref. 2). This diameter is not large enough to neglect the tunnel wall effect.

Figure 9 compares the DSMC and Navier–Stokes velocity fields, which are generally in agreement again, although there are some slight differences in detail. Figure 10 shows the DSMC and slip Navier–Stokes surface pressure coefficient profiles, which compare well to each other. In contrast to the supersonic condition (Fig. 4), the surface pressure is lower than the freestream pressure on most of the airfoil surface. This is caused by the increased viscous effect.

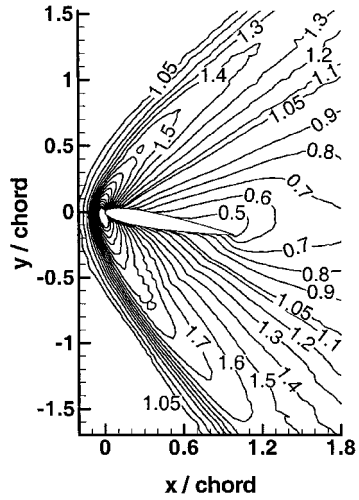

a) DSMC

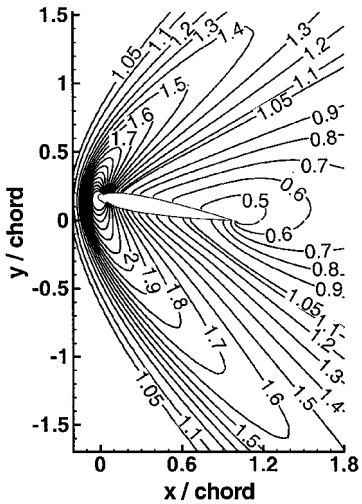

b) Slip N–S

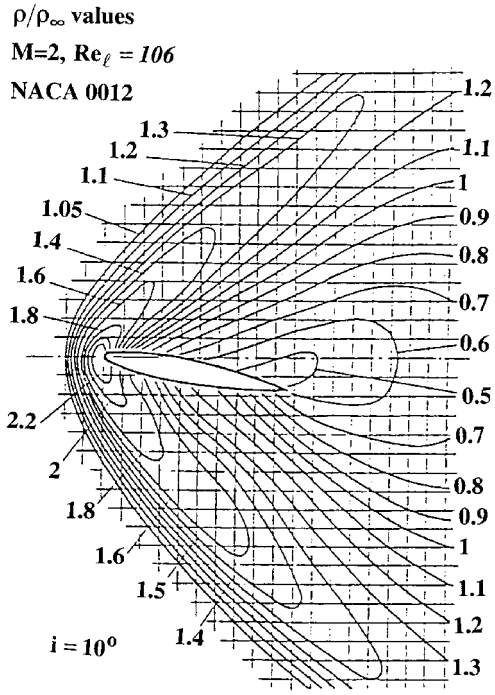

c) Experiment[2]

Fig. 5 Comparison of DSMC, slip N–S, and experimental density fields (ρ/ρ_∞) for case B.

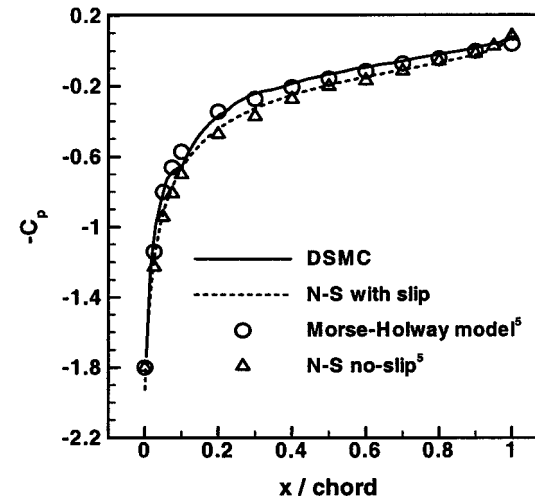

Fig. 6 Comparison of DSMC and slip N–S surface pressure distributions for case B.

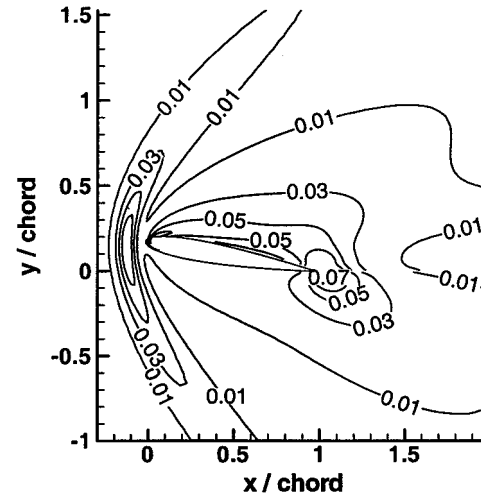

Fig. 7 Contours of GLL Knudsen number for case B.

Case D: $M_\infty = 0.1, Re_\infty = 10^1, \alpha = 0$ Degrees

Because the thermal velocity is much larger than the bulk flow velocity, and because of the very small variation in the flow properties, case D presents a serious challenge for the particle approach. Large numbers of cells and weighting factors have to be used to resolve the flowfield and surface properties. It is impossible for the flowfield to be separated from statistical noise using the DSMC method even by building up an enormous sample in each cell. Therefore, the particle calculation employs the IP technique, discussed earlier, to obtain macroscopic quantities.

The particle simulation starts from a uniform flowfield with about 60 simulated molecules per cell. The cells are concentrated around the airfoil. The cell size gradually increases from $L_c/43$ in the region adjacent to the airfoil surface to $L_c/8$ distant from the airfoil. A weighting factor scheme[9] is used to distribute the number of simulated molecules uniformly over the cells. The weighting factor of each cell is inversely proportional to its volume. After 15,000 time steps that take about 70 CPU hours on a SGI OCTANE workstation, the flow reaches a steady state. The IP results are then obtained through a further 1500 time steps of sampling.

Figures 11a and 11b compare the IP and slip Navier–Stokes density and velocity fields. There is a line near the leading edge and almost perpendicular to the airfoil along which the density is equal to the freestream value. In a region around the leading edge, the density increases due to the body and reaches a maximum at the leading edge. The flow expands from the front one-sixth of the airfoil, which causes the density to decrease to a minimum at the trailing edge. The total variation of density is very small, only about 3% of the

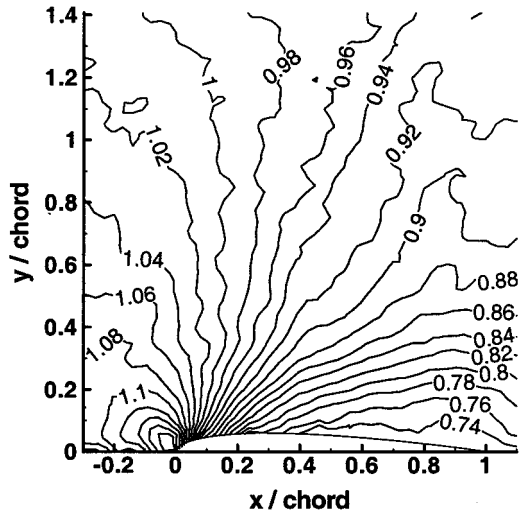

a) DSMC

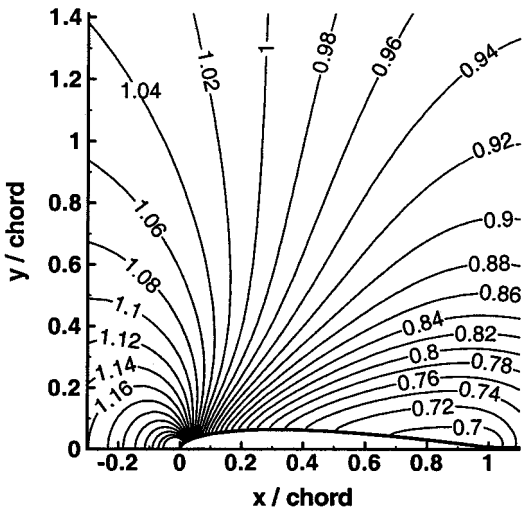

b) Slip N–S

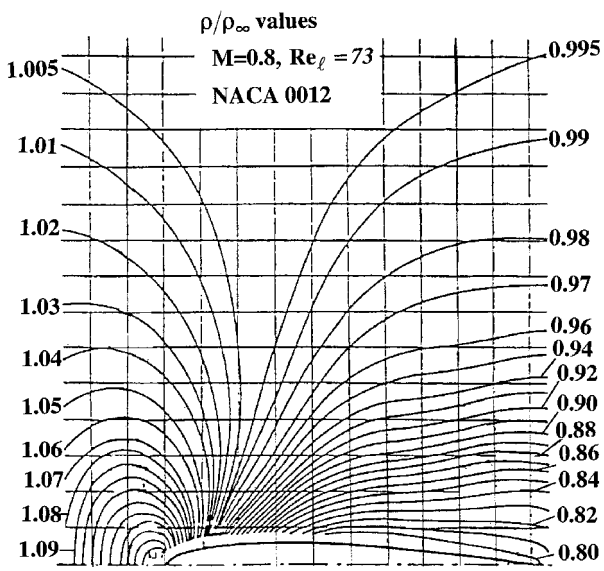

c) Experiment[2]

Fig. 8 Comparison of DSMC, slip N–S, and experimental density fields (ρ/ρ_∞) for case C.

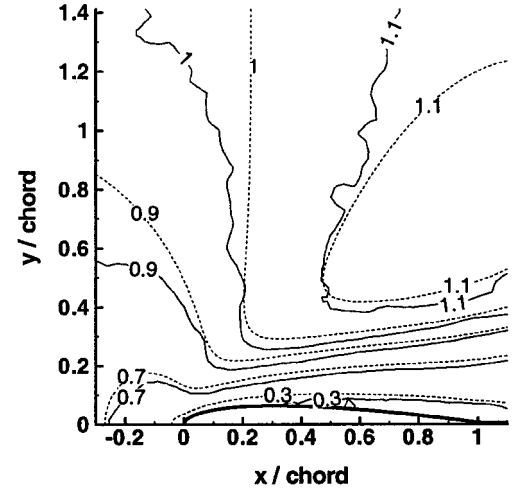

Fig. 9 Comparison of DSMC (——) and slip N–S (– – –) velocity distributions V/V_∞ for case C.

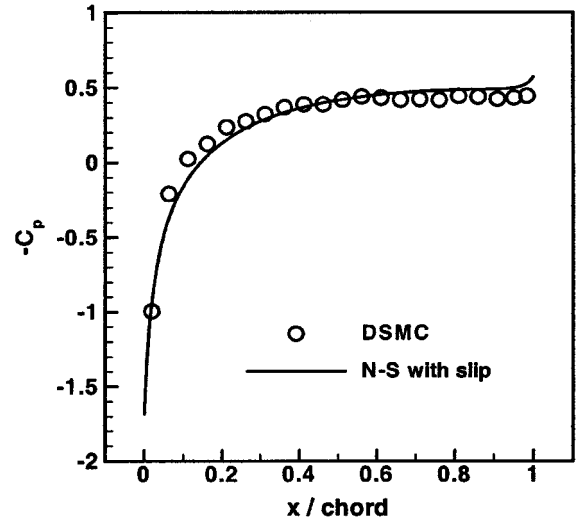

Fig. 10 Comparison of DSMC and slip N–S surface pressure distributions for case C.

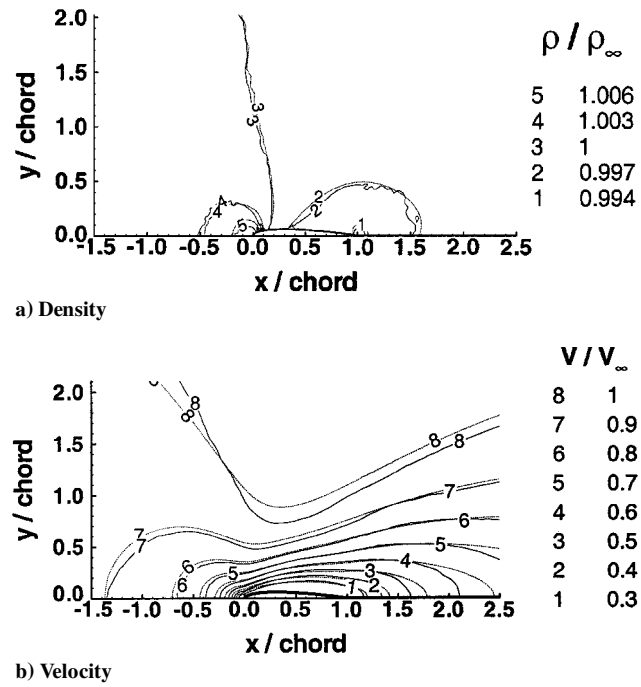

a) Density

b) Velocity

Fig. 11 Comparison of IP (——) and slip N–S (– – –) flowfields for case D.

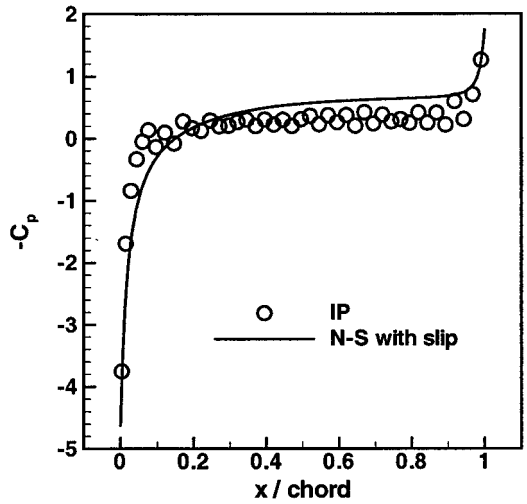

Fig. 12 Comparison of IP and slip N–S surface pressure distributions for case D.

freestream value. The IP results successfully resolve this variation and are in overall agreement with the slip Navier–Stokes solutions. The IP velocity field compares well with the slip Navier–Stokes velocity field, with a slight difference occurring in a region around the trailing edge.

Figure 12 compares the IP and slip Navier–Stokes surface pressure distributions. Both of them show that there is a sharp increase in pressure close to the leading edge, as expected. However, there is an interesting phenomenon at the trailing edge where the pressure is seen to decrease. This is not observed in high Reynolds number flows where a recompression is expected with a corresponding increase in pressure. Such a difference certainly results from the viscous effect that dominates this low Reynolds number flow and indicates that simply scaled-down versions of conventional airfoils perhaps do not provide optimum aerodynamic features.

Conclusions

Rarefied gas flows over a NACA 0012 airfoil were investigated using particle and continuum approaches. The flow conditions were varied from supersonic, to transonic, to low subsonic. The continuum approach solved the Navier–Stokes equations with a slip boundary condition on the airfoil surface, whereas the particle approach employs the DSMC method for the supersonic and transonic cases and the IP method for the low subsonic case. The DSMC and slip Navier–Stokes density and velocity fields for the supersonic and transonic cases were compared with experimental data, and good overall agreement was achieved. The particle and continuum surface pressure coefficients compared well for all of the cases and showed some interesting behavior resulting from the low Reynolds number conditions.

In terms of the particle methods, the DSMC method was found to perform with physical accuracy and numerical efficiency only for the supersonic cases. As the velocity was decreased to a transonic condition and then a low subsonic condition, the DSMC method encountered increased difficulties with high levels of statistical scatter. This scatter was significantly reduced through use of the IP technique. This technique was found to perform well for the subsonic case, although further refinements are still required.

Acknowledgments

The authors gratefully acknowledge support for this work from the Air Force Office of Scientific Research through Multidisciplinary Research Program Grant F49620-98-1-0433 to the University of Minnesota. Computer time was provided by the Minnesota Supercomputing Institute.

References

[1]Wilson, J. R., "Mini Technologies for Major Impact," *Aerospace America*, May 1998, p. 36.

[2]Allegre, J., Raffin, M., and Lengrand, J. C., "Experimental Flowfields Around NACA 0012 Airfoils Located in Subsonic and Supersonic Rarefied Air Streams," *Numerical Simulation of Compressible Navier–Stokes Flows*, edited by M. O. Bristeau, R. Glowinski, J. Periaux, and H. Viviand, Friedr. Vieweg and Sohn, Braunschweig, Germany, 1985, pp. 59–68.

[3]Allegre, J., Raffin, M., and Gottesdient, L., "Slip Effect on Supersonic Flowfields Around NACA 0012 Airfoils," *Rarefied Gas Dynamics 15*, edited by V. Boffi and C. Cercigani, 1986, pp. 548–557.

[4]Hasse, W., "Solution of the Navier–Stokes Equations for Sub- and Supersonic Flows in Rarefied Gases," *Numerical Simulation of Compressible Navier–Stokes Flows*, edited by M. O. Bristeau, R. Glowinski, J. Periaux, and H. Viviand, Friedr. Vieweg and Sohn, Braunschweig, Germany, 1985, pp. 139–157.

[5]Yang, J. Y., Huang, J. C., and Wang, C. S., "Nonoscillatory Schemes for Kinetic Model Equations for Gases with Internal Energy States," AIAA Journal, Vol. 34, No. 10, 1996, pp. 2071–2081.

[6]Bhatnagar, P. L., Gross, E. P., and Krook, M., "A Model for Collision Processes in Gases. I. Small Amplitude Processes in Charged and Neutral One Component Systems," *Physical Review*, Vol. 94, No. 3, 1954, pp. 511–525.

[7]Morse, T. F., "Kinetic Models for Gases with Internal Degrees of Freedom," *Physics of Fluids*, Vol. 7, No. 2, 1964, pp. 159–169.

[8]Holway, L. H., "New Statistical Models for Kinetic Theory: Methods of Construction," *Physics of Fluids*, Vol. 9, No. 9, 1966, pp. 1658–1673.

[9]Bird, G. A., *Molecular Gas Dynamics and the Direct Simulation of Gas Flows*, Clarendon, Oxford, 1994.

[10]Fan, J., and Shen, C., "Statistical Simulation of Low-Speed Unidirectional Flows in Transition Regime," *Rarefied Gas Dynamics*, Vol. 2, edited by R. Brun, Cepadues, Toulouse, France, 1999, p. 245.

[11]Oran, E. S., Oh, C. K., and Cybyk, B. Z., "Direct Simulation Monte Carlo: Recent Advances and Application," *Annual Review of Fluid Mechanics*, Vol. 30, 1998, pp. 403–441.

[12]Harley, J. C., Huang, Y., Bau, H. H., and Zemel, J. N., "Gas Flow in Microchannels," *Journal of Fluid Mechanics*, Vol. 284, 1995, pp. 257–274.

[13]Pong, K. C., Ho, C. M., Liu, J. Q., and Tai, Y. C., "Non-Linear Pressure Distribution in Uniform Microchannels," *Application of Microfabrication to Fluid Mechanics*, Fluid Dynamics Div., Vol. 197, American Society of Mechanical Engineers, Fairfield, NJ, 1994, pp. 51–56.

[14]Arklic, E. B., "Measurement of the Mass Flow and Tangential Momentum Accommodation Coefficient in Silicon Microchannel," Ph.D. Dissertation, Fluid Dynamics Research Lab., Dept. of Aeronautics and Astronautics, TR 97-1, Massachusetts Inst. of Technology, Cambridge, MA, 1997.

[15]Bird, G. A., "Monte Carlo Simulation in an Engineering Context," *Rarefied Gas Dynamics*, Vol. 74, Progress in Astronautics and Aeronautics, AIAA, New York, 1981, pp. 239–255.

[16]Vincenti, W. G., and Kruger, C. H., *Introduction to Physical Gas Dynamics*, Wiley, New York, 1965, p. 424.

[17]MacCormack, R. W., "Current Status of the Numerical Solutions of the Navier–Stokes Equations," AIAA Paper 85-0032, 1985.

[18]MacCormack, R. W., and Candler, G. V., "The Solution of the Navier–Stokes Equations Using Gauss–Seidel Line Relaxation," *Computers and Fluids*, Vol. 17, No. 1, 1989, pp. 135–150.

[19]Schaaf, S. A., and Chambre, P. L., *Flow of Rarefied Gases*, Princeton Univ. Press, Princeton, NJ, 1966.

[20]Dietrich, S., and Boyd, I. D., "Scalar and Parallel Optimized Implementation of the Direct Simulation Monte Carlo Method," *Journal of Computational Physics*, Vol. 126, No. 2, 1996, pp. 328–342.

[21]Alexander, F. J., Garcia, A. L., and Alder, B. J., "Cell Size Dependence of Transport Coefficients in Stochastic Particle Algorithms," *Physics of Fluids*, Vol. 10, No. 6, 1998, p. 1540.

[22]Alexander, F. J., Garcia, A. L., and Alder, B. J., "Erratum: 'Cell Size Dependence of Transport Coefficients in Stochastic Particle Algorithms,'" *Physics of Fluids*, Vol. 12, No. 3, 2000, p. 731.

[23]Boyd, I. D., Chen, G., and Candler, V. C., "Predicting Failure of the Continuum Fluid Equations in Transitional Hypersonic Flows," *Physics of Fluids*, Vol. 7, No. 1, 1995, pp. 210–219.

K. Kailasanath
Associate Editor